International Journal of Civil, Structural, Environmental and Infrastructure Engineering Research and Development (IJCSEIERD)
ISSN(P): 2249-6866; ISSN(E): 2249-7978
Vol. 5, Issue 4, Aug 2015, 53-72

STRUCTURAL BEHAVIOR OF DEEP REINFORCED CONCRETE BEAMS UNDER INDIRECT LOADING CONDITION

YOUSIF JABBAR LAFTA[1]&KUN YE[2]

[1,2]School of Civil Engineering, andMechanics, Huazhong University of Science and Technology, Wuhan, China

[1]Department of Civil Engineering, University of Basra, Ministry of Higher Education, Iraq

ABSTRACT

This study investigates the structural behavior of indirectly loaded deep reinforced concrete (RC) T-beams. A total of 21deep RC T-beams were divided into three groups according tothe ratio of shear span to effective depth. Beams without web reinforcement were tested under indirect point loading applied via central intersecting members until shear failure. Experimental results indicate that indirectly loaded deep beams can carry additional load after diagonal cracking is initiated. The performance of these beams is associated with 3Dnon-linear finite element analysis that involves discrete reinforcement modeling. This modeling process isperformed using ANSYS 12.1. Appropriate numerical modeling approaches are recommended, experimental load-deflection responses are compared in relation with FEA. The behavior of beams was observed under loading. Ultimate loads, deflection responses, and crack patternsare recorded as well. The numerical modeling results agreed with the test results for the beams.

KEYWORDS*:* Deep T-Beams, Indirect loading, Shear Span-To-Effective Depth Ratio

INTRODUCTION

The overall depth of reinforced concrete deep beam is considerably deeper than that of normal flexural members. Furthermore, the value of the thickness of deepermembers is significantly smaller than that of either depth or span. Winter[1], Park and Paulay[2],and Fereig and Smith [3] called members of this type deep beams. In such beams, the shear span/effective depth (a/d) ratio is less than 2 for simply supported beams and less than 2.5 for any span of continuous beams.Nawy[4]classified continuous RC beams with a/dratio not exceeding 2.0 to 2.5 as deep beams. American Concrete Institute Building Code 318-11[5]classified as deep beams those with clear spans that are less than or equal to four times the total depth of the members depth or whose support faces are subject to concentrated loads with values within twice the member depth, as well as beams that are loaded on one face and supported on the opposite face so that compression struts can develop between the loads and the supports. Two loading cases are encounteredby simply supported deep beams, namely, direct and indirect loading. In the former, external loads are applied perpendicular to the surface of a member in the direction of the member centroid (for example, traffic loadsacting to deck units).In the latter, external loads are applied to the sides of members and away from the centroid, as denoted by the headstocks that support beams onthe side faces of nibs[6].Deep RC beamshave been widelyused in high-rise buildingsas load-distributing structural partsof transfer girders, wall footing, foundation pile caps, floor diaphragms, and shear walls, among others.

Nonetheless, the performance of indirectly loaded deep RC beams is rarely investigated. Fereigand Smith [3]studied the behavior of indirectly loaded RCbeams with short shear spansunder loading and supporting

conditions.External loads are placed via shear brackets on the sides of the beams.Crack widths and deflections are more rarely encountered in direct loading than in indirect loading given beams with a/d = 0.5 or 1.0. Moreover, these widths and deflections are more often experienced during indirectly loading near the bottom than near the top. Beams with web reinforcement generallyexhibited narrow cracks, as well as few deflections and mild tensile steel strain.As per previous test results, arch action tendency was low for beams with a/d=2 than for beams witha/d= 0.5 and 1.0.Ferguson[7], Taylor [8], and Neville and Taub[9]performed experimentson short shear span beams underindirect loading conditions. In these experiments,a/dratiosare 1.35, 1.64, and 2.09 respectively. Theresults indicatethata large portion of the additional strength associated with small a/d ratioshas been lost.Similarly, Kalyanariman et al.[10]conducted experiments ontwo single-span deepbeams with flanges that were indirectly loaded via side arms.The tensile stress in steel was non-uniformly distributed over the length before diagonal tension cracks were formed.Once such cracks formed, this stress gradually became uniform because of the tied arch action commonly encountered in deep beams.The experimental results showed that the shear strength of indirectly loaded deep T-beams could bea maximum of 70% higher than that of indirectly loaded deep rectangular beams.Kong[11] andKalyanariman et al.[10]reported thatthe strong compression zone generated by the flanges in T-sections precludes shear compression failure in T-beams.As a result, shear strength capacity is increased.Many parameters affect the strength of deep beams,includinga/d ratio, loading and supporting conditions, the extent and arrangement of tensile and web reinforcement, beam proportion and shape, and concrete and steel properties.According to Mohammad[12], the failure behaviors of deep beams differ significantly from those of ordinary beams due to load transfer mechanismand geometry.The behavior of RC deep beams ($a/d \leq 2$ [13]) loaded in shear conditions also varies from that of shallow beams because of the arch action initiated after diagonal cracking.Denpongpan[14]also concluded that RCdeep beams without shear reinforcement can bearshear force through thisaction, in which load is transferred directly to the support via diagonal compressive strut.As per the experimental works conducted by several researchers [7],[15], and[16], themechanical behavior of indirectly loaded deep beamsdiffers from that of directly loaded deep beams.Furthermore, shear strength and shear at the firstdiagonal tension crack are much lower for indirectlyloaded deep beams than for directly loaded deep beams. This finding can be attributed to the lack of confining compressive forces in indirectly loaded deep beams.

In the presentstudy, 21indirectly loaded deep RCT-beamswithout web reinforcementare subjected to point loads applied via inter section members in the centers of the beams. The mainvariables are flange size, the overall depthof the beams, and a/d ratio.Allof the tested beams fail in shear; nonetheless, no local failure is observed due to crushing of concrete under the loads or over the supports.During the testing period, cracks, strains, deflection, and ultimate loads are recorded. A detailed 3D finite element (FE) model of a typical deep RC T-beam under indirect loading is presented to evaluate shear performance, as well asto predict and validate the experimental test result obtained by the authors.Thisresearchis performedusing the non-linear FE software packageANSYSto predict ultimate indirect loading capacity and to estimate the curve of the load—mid-span deflection relation. Theaccuracy of the analysis is validated by comparing the ultimate load and deflection results generated by the FE model against the experimental results. In addition, the analysis yields important findings on the resistance of deep concrete beams with flanges that are affected by indirect loading conditions.The experimental results confirm previous findings reported by Zhang N, Tan, KH[17], which postulatethat the effect of beam depth significantly influencesthe shear capacity and ultimate load of deep beams. In summary, the experimental results indicated the significant effect of flange size and beam depth on the shear strength of deep, flanged RC beams under indirect loading.

EXPERIMENTAL PROGRAM

Specimen Details

A total of 21 simply supported,single-span deep concrete beamsare divided into three groups witha/d ratios of 1.0, 1.4, and 1.8. Each group consists of seven specimens;sixhad an overall height (h) of 300mm,whereas the remaining specimen was 400mm high. All of T-cross section beams exhibited a web thickness (b_w)of 120mm; flange widths (b_f) of240,300, and 360 mm; and flange depths (h_f)of 60and 90 mm.The specimensalso contain rectangular central intersecting member with the same overall depth as the beams depth (300mm). The width is (120 mm) and length isequal to the flange width of the beams. The beams are tested to failure under indirect point loads on the mid-span. The details and dimensions of the beams are provided in Table 1 and in Figure 1. All main beams are single span withoutshear reinforcement. The beams are designed to fail in shear; suitable tension reinforcement is provided to prevent flexural failure. The design compressive strength is obtainedfor cylindricalspecimens with dimensions of 300 mm (height)× 150 mm (diameter) in accordance with standard C 39 of the American Society for Testing and Materials [18].The value of fc′ is derived from the mean values of three concrete cylinders cured under the same conditions for 28 days and tested on the same day of the specimenstesting. The measured compressive strength of the employed concreteis 25MPa, and the slump is approximately 120 mm[10, 19]. Two types of reinforcement are usedin the specimens, namely, a deformed steel rebar for longitudinal reinforcement and a plain roundsteel rebar for flange and web reinforcement of intersecting member.The main reinforcement isprovided by deformed steel bars with a diameter of 12 mm withyield strength of 270 MPa. The bars are anchored behind the support with sufficient length[20]and with a 90° bent to prevent anchorage zone failure.Stirrups with a diameter of 6mm arelocated at the supportsof the RC T-section beams and at the areas on which loads are applied. The material properties of stirrups and the main reinforcement are shown in Table (2). The values are averaged from three 600-mm long steel bars.Bearing plates that are 120mm wide, 10mm thick, and 120mm longare positionedat the loading and supporting points to prevent local crushing failure in the concrete,as illustrated in Figure2.The specimen notation is typically written as “TB1Gr1”, where TB1 is the number of beams in the series of TB1, TB2, … TB7 and character (Gr1, Gr2, and Gr3) denotes the a/d ratios of 1.0, 1.4, and 1.8,of the three groups.

Instrumentation and Test Setup

The typical experimental setups and arrangement for tested beams aredisplayed in Figures 3 and 4. A steel spreader beam controls the two equal point loads. This beam is situated on a two-pin support that is placed on top of the beams.Torsee’s Universal Testing Machine was used to apply the load; this machine has a capacity of 2000 kN.Mid-span deflections aremeasured by anaccuracy dial gauge (ELE type) with 0.01 mm accuracy.A capacity of30mm is assigned to the area underneath the center ofthe bottom faces of the specimens.The beamsare loaded from top via the intersecting member at the center of the span of the beams. Load was applied incrementally; at each increment, the total load applied to the beam, the mid-span deflection, and the crack width are measured. Specifically, crack width is measured using a hand microscope, plotted, and marked.The test is terminated when the total load on the specimens begins tocollapse.

Table1: Details of the Tested Beams

Beam No.	a/d	L/h	h_f mm	b_f mm	f_c' MPa
Series 1					
TB1Gr1	1.0	1.67	60	360	25
TB2Gr1	1.0	1.67	90	360	25.6
TB3Gr1	1.0	1.67	60	300	28
TB4Gr1	1.0	1.67	90	300	27
TB5Gr1	1.0	1.67	60	240	25.5
TB6Gr1	1.0	1.67	90	240	27.5
TB7Gr1	1.0	1.75	60	360	25.6
Series 2					
TB1Gr2	1.4	2.30	60	360	26.7
TB2Gr2	1.4	2.30	90	360	28.5
TB3Gr2	1.4	2.30	60	300	26
TB4Gr2	1.4	2.30	90	300	25.4
TB5Gr2	1.4	2.30	60	240	25.7
TB6Gr2	1.4	2.30	90	240	25.8
TB7Gr2	1.4	2.45	60	360	25
Series 3					
TB1Gr3	1.8	3.00	60	360	25.4
TB2Gr3	1.8	3.00	90	360	25.2
TB3Gr3	1.8	3.00	60	300	25.8
TB4Gr3	1.8	3.00	90	300	25.9
TB5Gr3	1.8	3.00	60	240	26.4
TB6Gr3	1.8	3.00	90	240	27.3
TB7Gr3	1.8	3.15	60	360	25.6

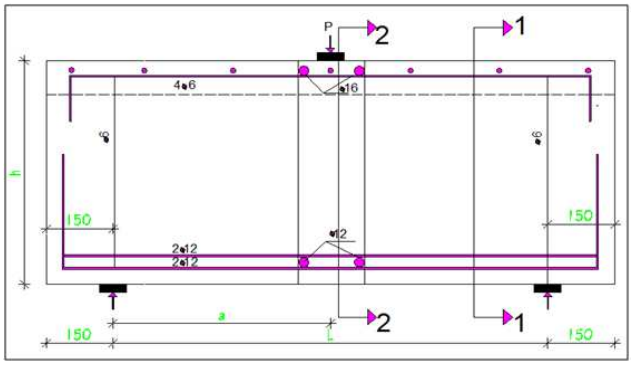

(a)

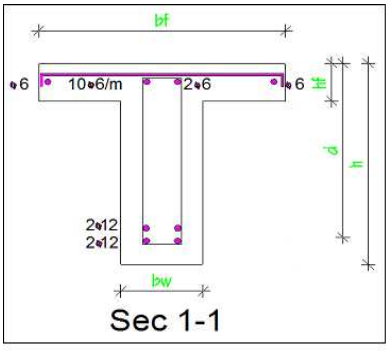

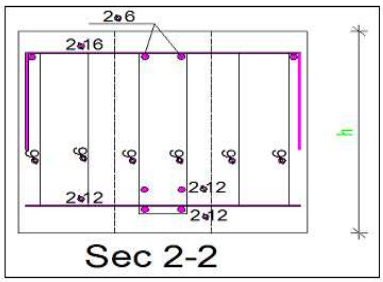

(b) **(c)**

Figure 1: Details of Tested Beams, B. Section in Main Beam, C. Section in Inter Section Beam

Table2: Material Properties of the Rebar and Stirrups

Type	Yield Strength (MPa)	Ultimate Strength (MPa)	Modulus of Elasticity (MPa)
D6	450	560	200000
D12	330	520	200000
D16	330	600	200000

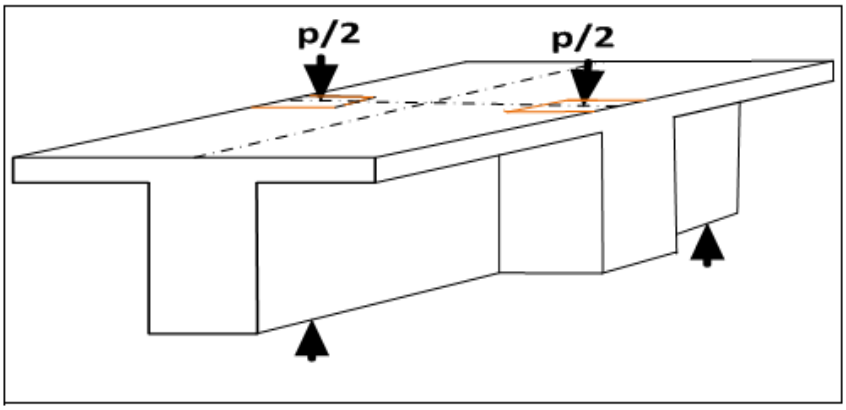

Figure 2: Indirect Point Loads

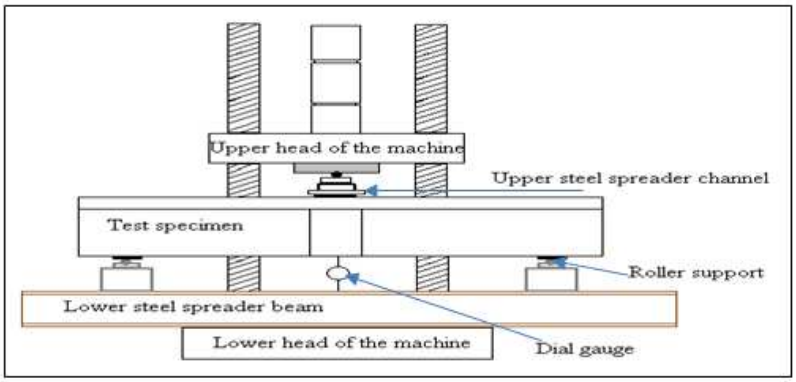

Figure 3: Test setup

Figure 4: Test arrangement

EXPERIMENTAL RESULTS

Behavior of Beams Underloading and Crack Patterns

The crack patterns of the three series of specimens showed that a significant part of the load is transferred to support through compression struts as shown in figure 5.This load transfer mechanism inducesa common type of failure in deep beams [12, 21].Figure 5 presents crack patterns,observed that when the load is increasedinclined cracks developed in the shear span region. After internal forces are redistributed thebeams sustain the additional load through arch action.All of the tested beams fail in shearwhen the diagonal shear cracks widen. Nonetheless, no local failure is observed due to the crushing of concrete under the load or over the supports. The main bars are provided with adequate end anchorage.Therefore, no anchorage failure is encountered during testing. In beams with a/d ratio of 1.0, the first diagonal crack is generated with a thud between the applied load and the support at mid-depth. Moreover,a few fine, inclined cracks are observed at the mid-depthof the loading path that is transmitted to the support.These cracks do not bridge with one another. A major inclined crack is widened at failure load.Beams with a/d ratios of 1.4 and 1.8 display similar behavior; however, the formation of inclined cracks is preceded by the development of a few inclined cracks near the intersecting member at the bottom of the mainbeams. Failure was suddenly induced by the extension of the diagonal crack through the compression flange.

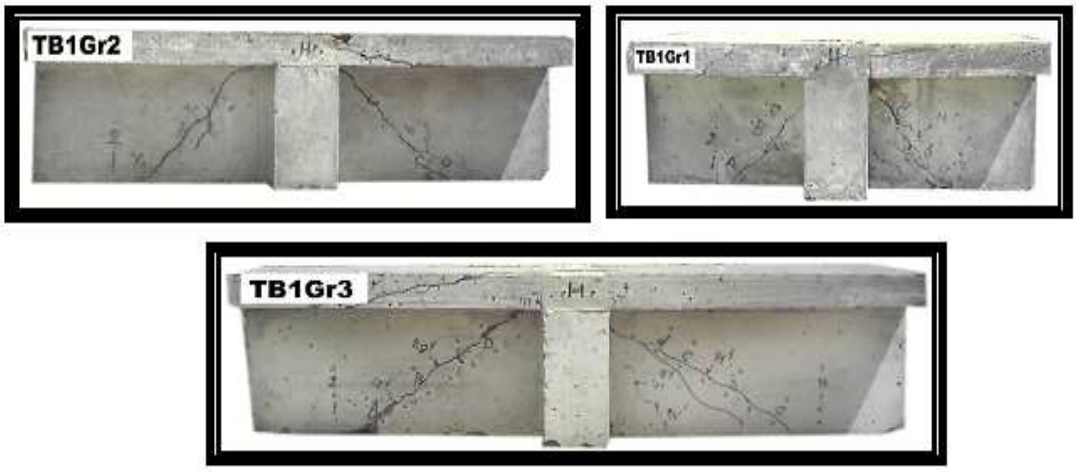

Figure 5: Crack Pattern of Test Beams

InclinedCracking and Ultimate Loads

The inclined crackingand ultimate loads are listed in Table 3. The former is defined as the load at which the first major inclined crackis initiated in the shear span.When inclined cracks are generated, deep beams develop tied arch behavior (arch action). This behavior can improve the shear strength of such beams[21].In group (1), beams TB2, TB4, and TB6 exhibited 37%, 38%, and 10% higher ultimate loads, respectively, than beams TB1, TB3, and TB5.In group (2), beams TB2, TB4, and TB6 reported 10%, 15%, and 26% higher ultimate loads, respectively, than beams TB1, TB3 and TB5.In group (3), beams TB2 and TB4 displayed 11% and 10% higher ultimate loads, respectively, than beams TB1 and TB3. Thisincrease in the ultimate loads of beams with high flange depth is attributed to the strong compression zone generated through increasing flange depth. The reservestrength of the beams is defined as the ratio of the difference in ultimate load and diagonal cracking load to diagonal cracking load[22]. This strength isexpressed as a percentage and measuresthe reservestrength beyond the inclined crackingload[23].This strength decreaseswhen a/d ratio increases,as

shown in Table 3.As per a comparison of the beams in groups 1, 2, and 3,ultimate load-carrying capacity increases by 67% in beams with flanges that are 60mm deep and 360mm wide when a/d ratio is reduced from 1.8 to 1.0.This capacity increases by 80%in beams with flanges that are 90mm deep and 360mm wide. The other beams exhibit similar behavior. This increase is attributed to the increased contribution of arch action-inducedshear transfer in beams with low a/d ratio and is evidentwhen flange depth increases as shown in Figure6. Figure 7displays the effect of beam depth on the shear strength ofthe three groups.Shear stress notably decreases with an increase in beam depth. Figure 8 presentsthe loads versus crack width for the three groups. Crack width increasessuccessively during testing. At the same load level, beams with deep flangesexhibit narrower cracks than beams with shallow flanges.The same tendency is observed with the effect of overall depth; however,the opposite tendency is noted for a/d ratio. Flange width exerts a weak effect on the widths of major inclined cracks.

Effect of Flange Depth

Table (3) shows that maximumload-carrying capacity increaseswith flange depth (in the same group). To eliminate the effects of the variation in concrete compressive strength on ultimate loads, non-dimensional quantity ($Pu/bhf_c' = R$) was calculated and the results included in Table (3). As illustrated in Figure 9, beams with similar flange width and 90-mm deep flanges exhibited increased ultimate loads (with the same a/d ratio).This increase is attributed to the strong compressive zone generated by the increase in flange depth. Beams TB2Gr1, TB4Gr1, and TB6Gr1 display 34%, 3%, and 9% higher initial cracking load and 18%, 15%, and 20% higher ultimate load than corresponding beams TB1Gr1, TB3Gr1, and TB5Gr1. In groups 2 and 3,the variation in flange depth more significantly affected ultimate load thanit did cracking loads.

Effect of a/dRatio

The inclined cracking and the subsequent failure of deep RC beams are strongly affected by the relative magnitudes of shearing and flexural stresses[24].This effect may be conveniently considered to be a function of a/d ratio. The distribution of stresses in the beams subject to indirect loading suggested a tendency toward arch action after cracking but not toward pure arch action because the force in the tension reinforcement is not constant through the span[10].The relations between (a/d) ratio and the measured ultimate load for tested beams are presented in Figure 6.Ultimate load is increased considerably by reducing the a/d ratio, because the property of arch action is low given a higha/d ratio[3].

Load-Deflection Response

The curves of load- versus mid-span deflection of the tested beams are plotted in groups and displayed in Figure 10.The slope of the curves changed after the inclined crack was formed, because the onset of the first major inclined crack reduced beam stiffness significantly.Beams with 90-mm deep flangesexhibit smaller deflectionsthanbeams with 60-mm deep flanges at the same load level and with the same a/d ratio. Moreover,400-mm deep beamsdisplay smaller deflections than 300-mm deep beams.An increase in flange width increases deflection,as observed in the three groups.

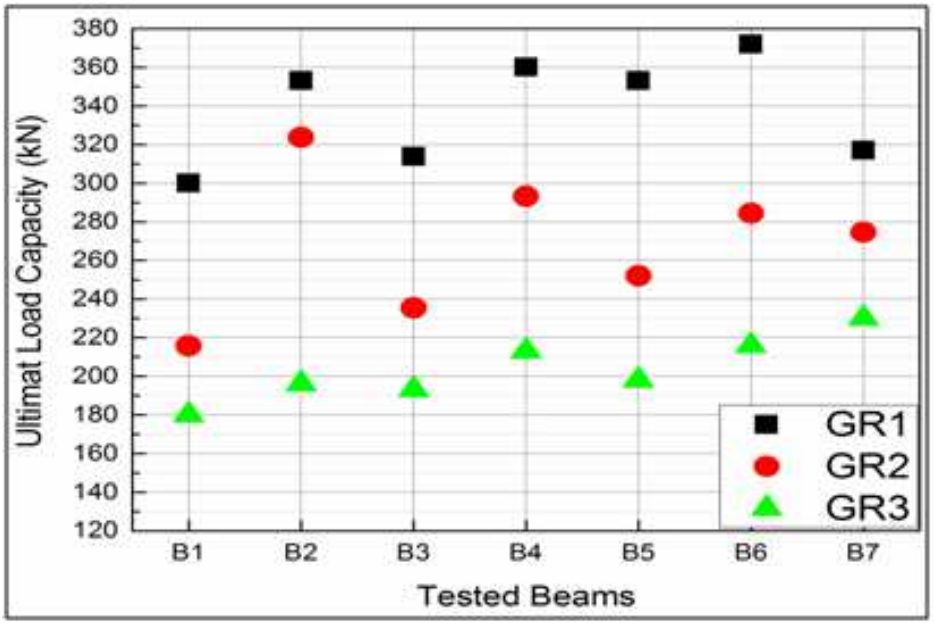

Figure 6: Ultimate Load-Carrying Capacity of the Tested Beams given Different a/d Ratios

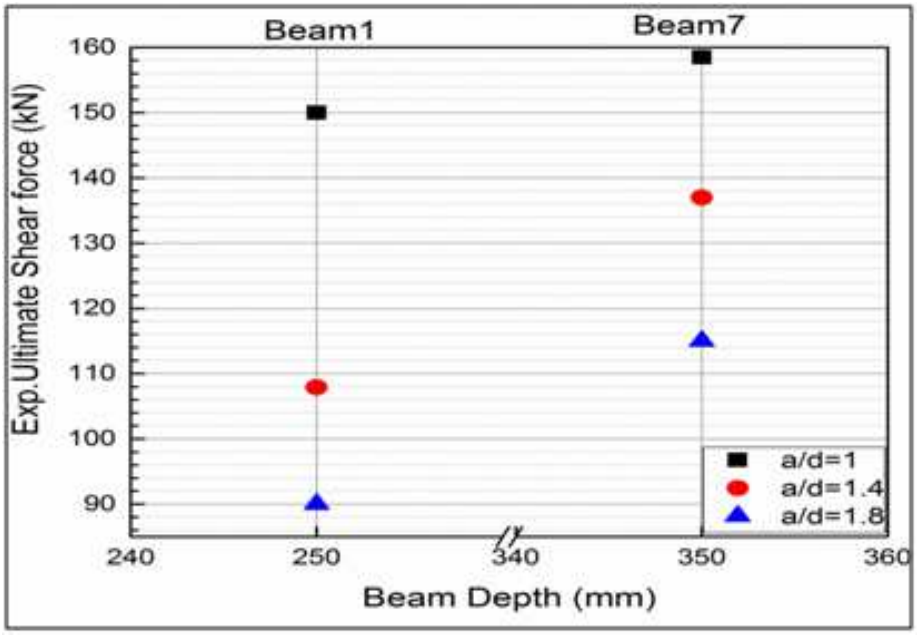

Figure 7: Effect of Beam Size in the Three Groups

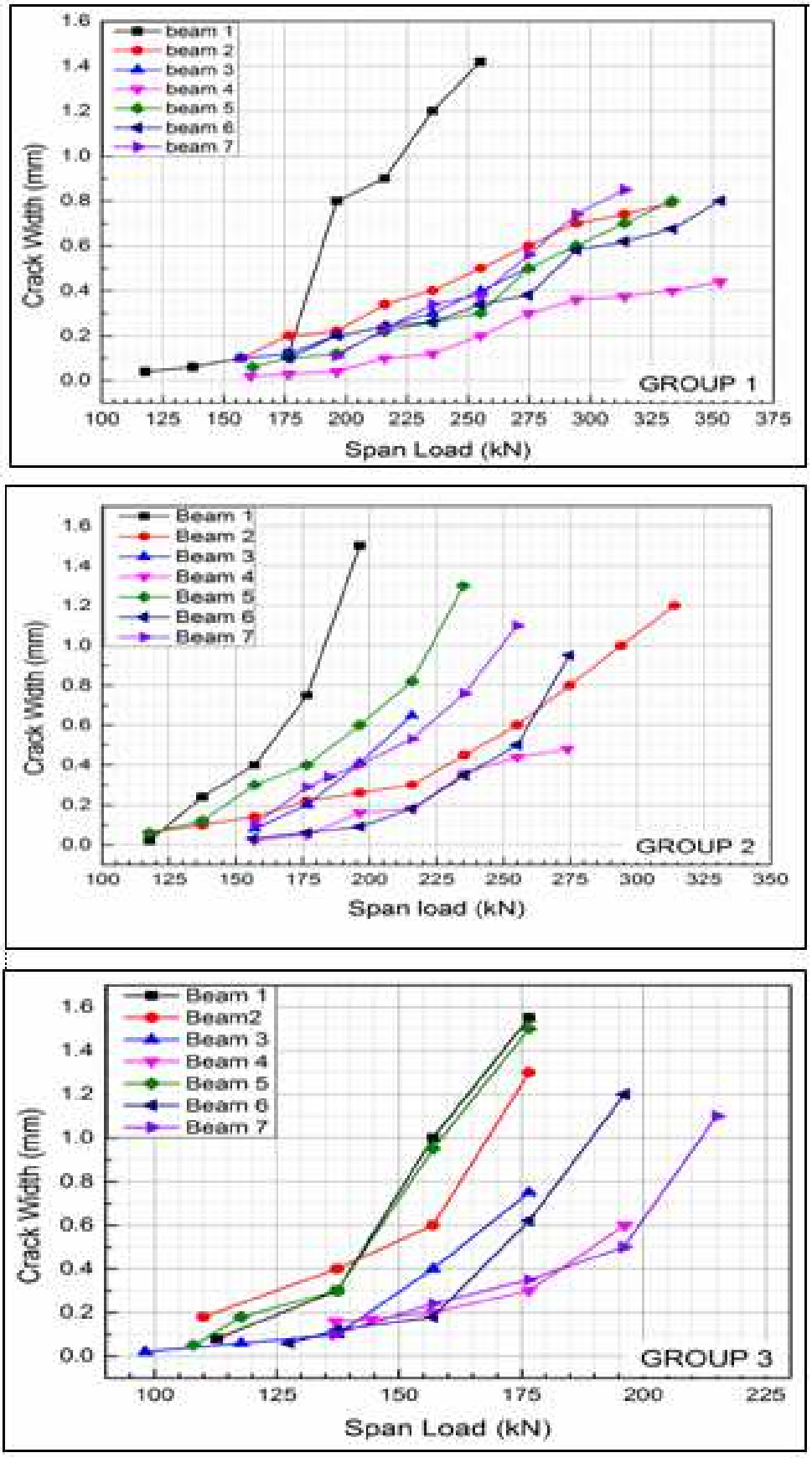

Figure 8: Load versus Crack Width in the Three Group

Table 3: Inclined Cracking and Ultimate Load in the Experiment

Beam no.	Span load (kN)		P_{cr}/P_u	P_u/bhf_c' (R)	$\frac{P_{U-}P_{cr}}{P_{cr}}\times 100$
	Inclined Cracking P_{cr}	Ultimate P_u			
Group (1) a/d = 1					
TB1Gr1	117.70	300.00	0.39	0.27	155%
TB2Gr1	156.96	353.00	0.44	0.37	125%
TB3Gr1	156.96	313.90	0.50	0.29	100%
TB4Gr1	160.96	360.00	0.45	0.40	124%
TB5Gr1	161.86	353.00	0.46	0.32	118%
TB6Gr1	176.95	372.78	0.47	0.35	111%
TB7Gr1	196.96	317.80	0.62	0.23	61%
Group (2) a/d = 1.4					
TB1Gr2	117.70	215.82	0.55	0.21	83%
TB2Gr2	117.70	323.73	0.36	0.23	175%
TB3Gr2	156.60	235.44	0.67	0.26	50%
TB4Gr2	156.96	293.32	0.54	0.30	87%
TB5Gr2	117.70	252.12	0.47	0.23	114%
TB6Gr2	156.60	284.50	0.55	0.29	82%
TB7Gr2	156.96	274.68	0.57	0.26	75%
Group (3) a/d = 1.8					
TB1Gr3	112.80	180.00	0.63	0.19	60%
TB2Gr3	110.00	196.00	0.56	0.21	78%
TB3Gr3	98.00	193.00	0.51	0.20	97%
TB4Gr3	137.00	213.00	0.64	0.22	55%
TB5Gr3	107.90	198.00	0.54	0.22	84%
TB6Gr3	127.50	215.80	0.59	0.22	69%
TB7Gr3	137.00	230.00	0.59	0.26	68%
		Average ratio	0.53		
		Standard dev.	0.08		

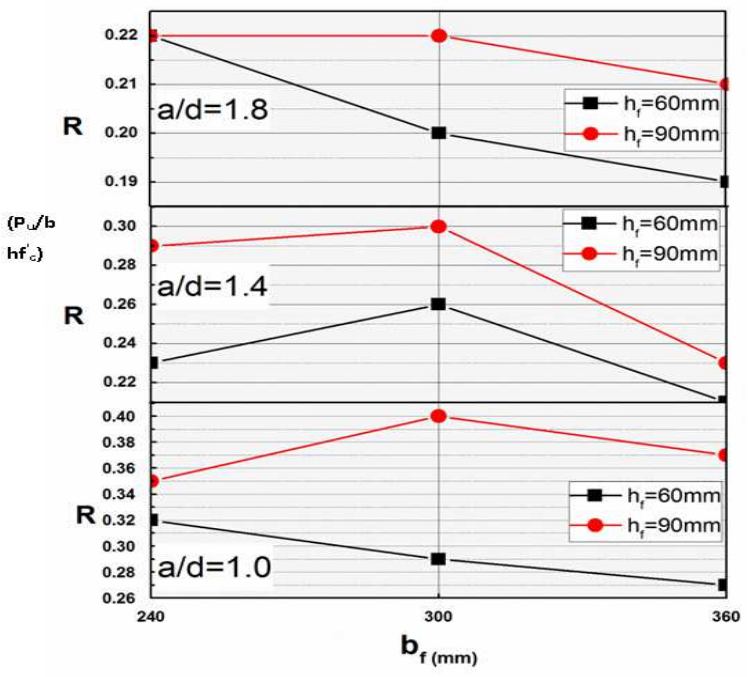

Figure 9: Effect of Flange Size on the Tested Beams

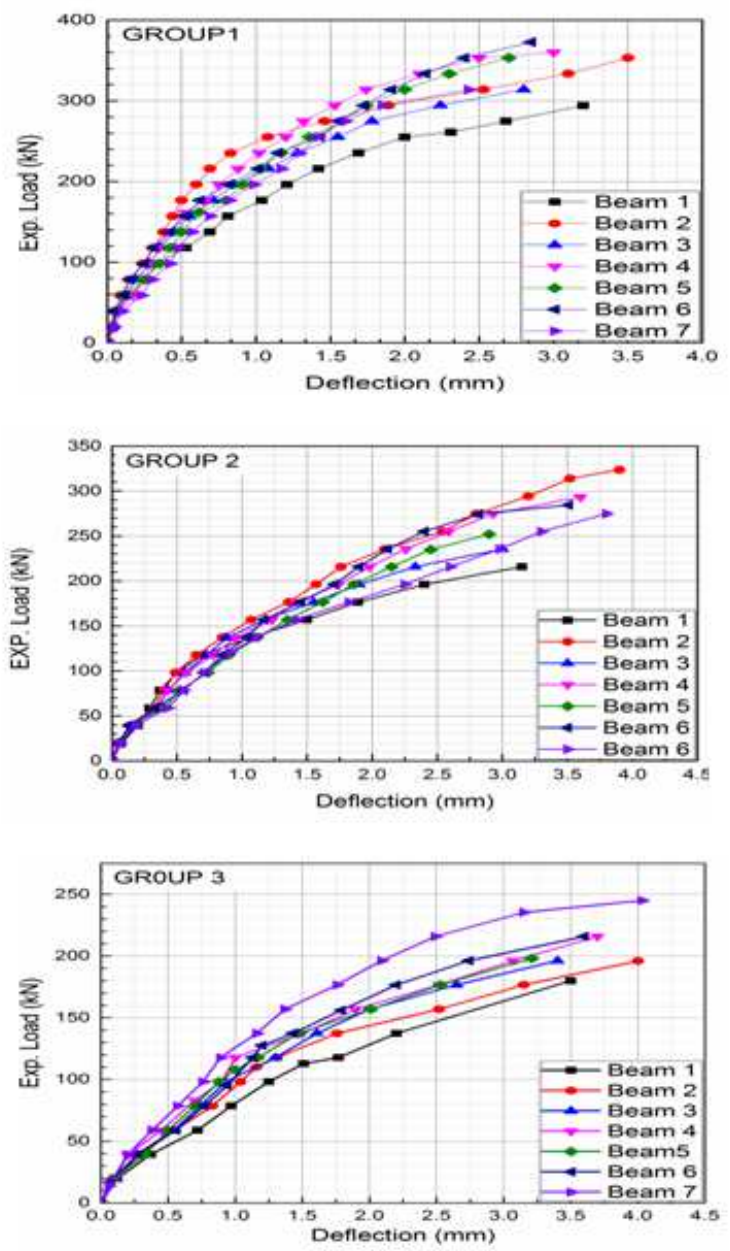

Figure 10: Load-Mid-Span Deflection of the Tested Beams

FINITE ELEMENT MODEL

The FE model considered in the current study has the same geometry, dimensions, and configuration as the test specimens. Table 1 shows the geometries of the models of the three groups of T-deep beams. The details are provided in Figures1 and2. FE analysis is performed using ANSYS 12.1 in the current study[25]. A quarter of the full beam was modeledaccording to the symmetry of the materials, loading, and boundary conditions. This model was analyzedon the basis of the code of commercial FE ANSYS [25]. The benefit of building quarter models of this construction is that the total number of elements is reduced to save much computational time. The selected element types in ANSYS 12.1[25], by Wolanski[26], and by Kachlakev[27]are the 3D 8-Node Reinforced Concrete Solid andthe structural element, SOLID65 to model concrete material for non-linear reactions of brittle materials on the basis of a constitutive model for concrete

triaxialbehavior.This element covers a smeared crack in tension zones and a crushing response in compression zones. The material used in steel reinforcement is a 3D two-node structural bar given the structural element LINK8. The supports and area at which loads are appliedon the steel plate are denoted by a 3D eight-node structural solidgiven structural element SOLID45. The models of the different materials were used by Wolanski[26], Kachlakev[27], Mohammed [28],and Hemmaty[29] for structural stress analysis.The FE model is shown in Figure 11.Concrete is modeledaccording to the standard non-linear constitutive material model of concrete implemented within ANSYS 12.1 software. This modelis based on the formulation developed by Williams and Warnke[30]. The non-linear response of a RC structure is commonly produced by three major factors: concrete cracking, concrete non-linearity in compression, and the plasticity of the steel reinforcement rebar. Prior to the formation of the first crack,the behavior of concrete is linear; afterward,this behavior becomes non-linear. The values of the coefficient of shear transfer across a crack varies between complete shear transfer and no shear transfer at the cracked section depending on the crack texture, as per Hemmaty[29].

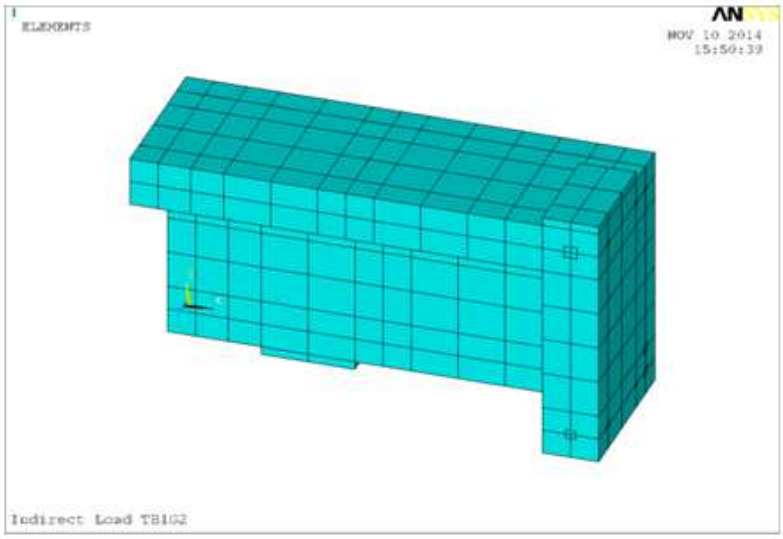

Figure 11: FE Model (Isometric of the FE Model of One Quarter of the Beam and Mesh)

Numerical expressions, that is,Equations(1), (2) [31], and (3) [32],were used to construct the uniaxial compressive stress—strain curve for compressed concrete used in the present study.

$$f = \frac{E_c \varepsilon}{1 + \left(\frac{\varepsilon}{\varepsilon_0} \right)^2} \quad \textbf{(1)}$$

$$\varepsilon_0 = \frac{2 f_c}{E_c} \quad \textbf{(2)}$$

$$E_c = \frac{f}{\varepsilon} \quad (3)$$

Where f = stress at any strain ε ; ε = strain at stress f ;and ε_0 = strain at ultimate compressive strength.

The first point of the curve must satisfy Hook's law in the implemented multilinear isotropic stress—strain relationship. Figure 12 shows the simplified compressive uniaxial stress—strain relationship that is considered in the current study[33].

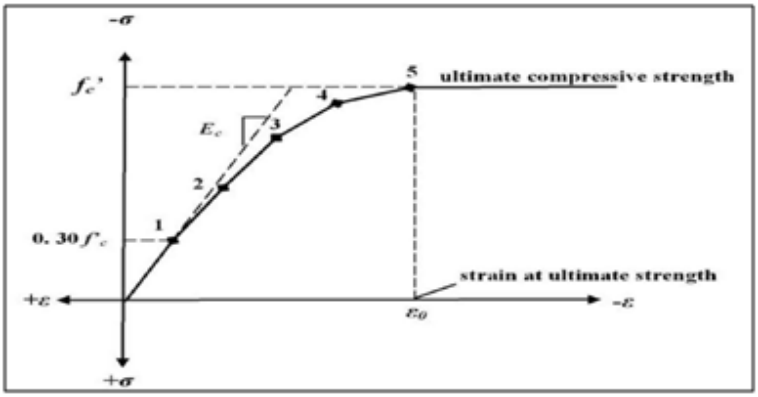

Figure 12: Simplified Compressive Uniaxial Stress Strain Relationship in Concrete

Inclined cracks first develop in beams with a/d ≤ 2.5.Once internal forcesare redistributed, the beams accommodate the additional load through arch action[20]. The tensile stress—strain response of concrete as a linear elastic relationship and the stiffening of RC tension after cracking are represented by a linearly descending branch until the point of cracking stress.The tension-stiffing effect is considered because the cracked concrete can still handle slight tensile stresses in the normal crack direction.Thisresult isgenerated in ANSYS by assuming the gradual release of the concrete stress component normal to the cracked plane[34].The relation of uniaxial stress versus strain for reinforcing steel rebarsisidealized as a bilinear curve.This curve represents elastic—plastic behavior with strain hardening. This relation is assumed to beidentical in terms of both tension and compression as per the European Committee's[35]criterion of von Mises plasticity yield. This scenariois displayed in Figure 13.

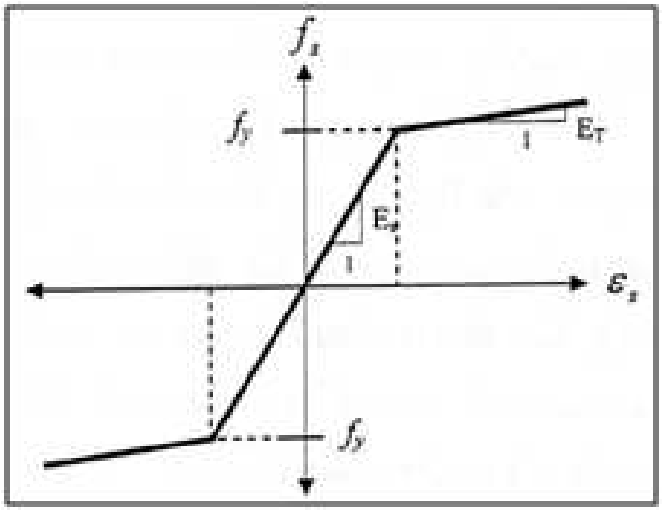

Figure 13: Modeling of Reinforcing Bars

Figure 14 depicts the typical 3D failure surface of concrete materials. The stress on this surface is biaxial or nearly

biaxial, and the most significant nonzero principal stresses are in the *x* and *y* directions [36]. When these principal stresses are both negative in value (compressive), the failure mode is a function of the sign of the principal stress in the *z* direction. Three failure surfaces can be generated as in Figure 14.The principal stresses in the *z* direction are slightly greater than zero (cracking), equal to zero (crushing), and slightly less than zero (crushing). When one or both of the principal stresses in the *x* and *y* directions are positive in value (tensile), the failure mode is cracking.This mode is illustrated in Figure 14 [36]. DuringFE analysis, cracking was induced in a concrete element when the principal tensile stress in any direction is observed beyond the failure surface. The elastic modulus of the concrete element is set to zero after cracking in the direction that is parallel to the direction of principal tensile stress. Crushing occurs whenall principal stresses are compressive and are beyond the failure surface [36]. Consequently, the elastic modulus is set to zero in all directions. Furthermore, the value of the local stiffness of the element becomes zero. This value inducessignificant displacement and, subsequently,divergence in the solution.

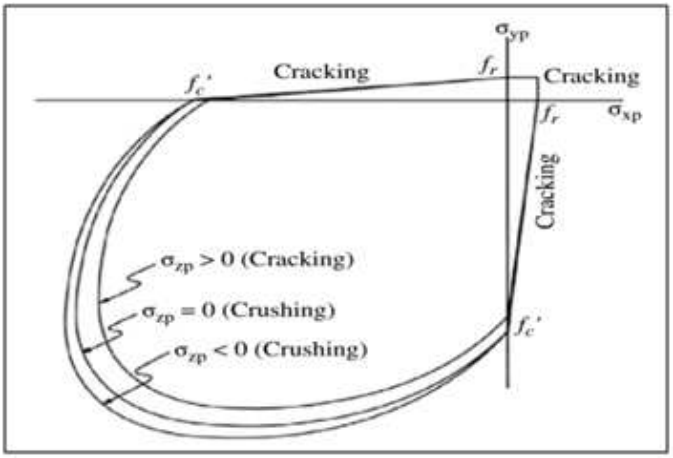

Figure 14: 3D Failure Surface for Concrete

In the current study, load is applied incrementally on a steel plate.The process is iterated toobtain a converged solution that corresponds to the loading stage under consideration. Newton—Raphson procedure is performed in full; the load is subdivided into increments of series loadsthat are applied in several steps.A stiffness matrix is formed at each iteration. This iterative procedure continues until a solution is convergent. The advantage of this procedure is that it may produce accurate results;nonetheless, the disadvantage liesin the significant computational effort that may be required to form and decompose the stiffness matrix.This scenario is presented in Figure 15. The beams and plates are modeled as volumes.

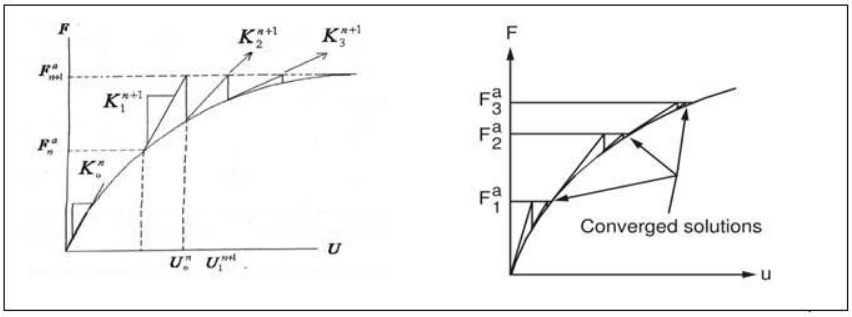

Figure 15: Incremental-Iterative Procedures and the Full Newton-Raphson Procedure

COMPARISON RESULTS

To assess the validity and predictability of the model, the experimental results are compared with the FE findings. Figure 16 shows typical measured and analyzed results predicted using FE ANSYS with the respect to the mid-span vertical displacement at the centerline of the cross section versus the applied indirect load. The advantage of the FE model is reflected by the fact that the numerical mid-span deflection is very close to the experimental data when all factors are well controlled. The curve of FE load-deflection response differs slightly from the experimental curve;this discrepancy may be explained by certain effects. First, micro cracks are existent in the tested concrete beams andcan be formed through drying shrinkage in the concrete and/or beam handling. By contrast, the non-linear FE models do not contain micro cracks. Second, the bond between the concrete and steel reinforcement is assumed to be perfect in the FE analysis. However, this assumption is not true for the tested beams.

Figure 17presents the crack patterns of the ANSYS models for comparison with those of the test beams. Figures 16 and 17clearly indicate that the experimental results agree with the numerically predicted FE deflection findings. Although the model of nonlinear numerical analysis under-predicts the ultimate load carrying capacity slightly,the study results confirm the experimental and FE analysis results presented by Özcan et al.[37].

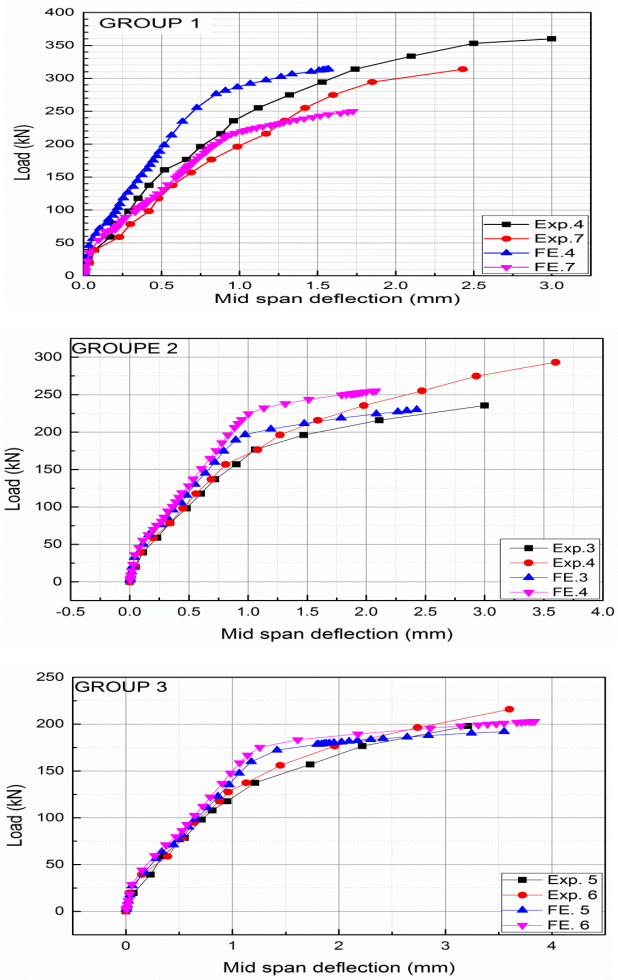

Figure 16: Load Versus Mid- Span Deflection Comparison between Experimental and FEA

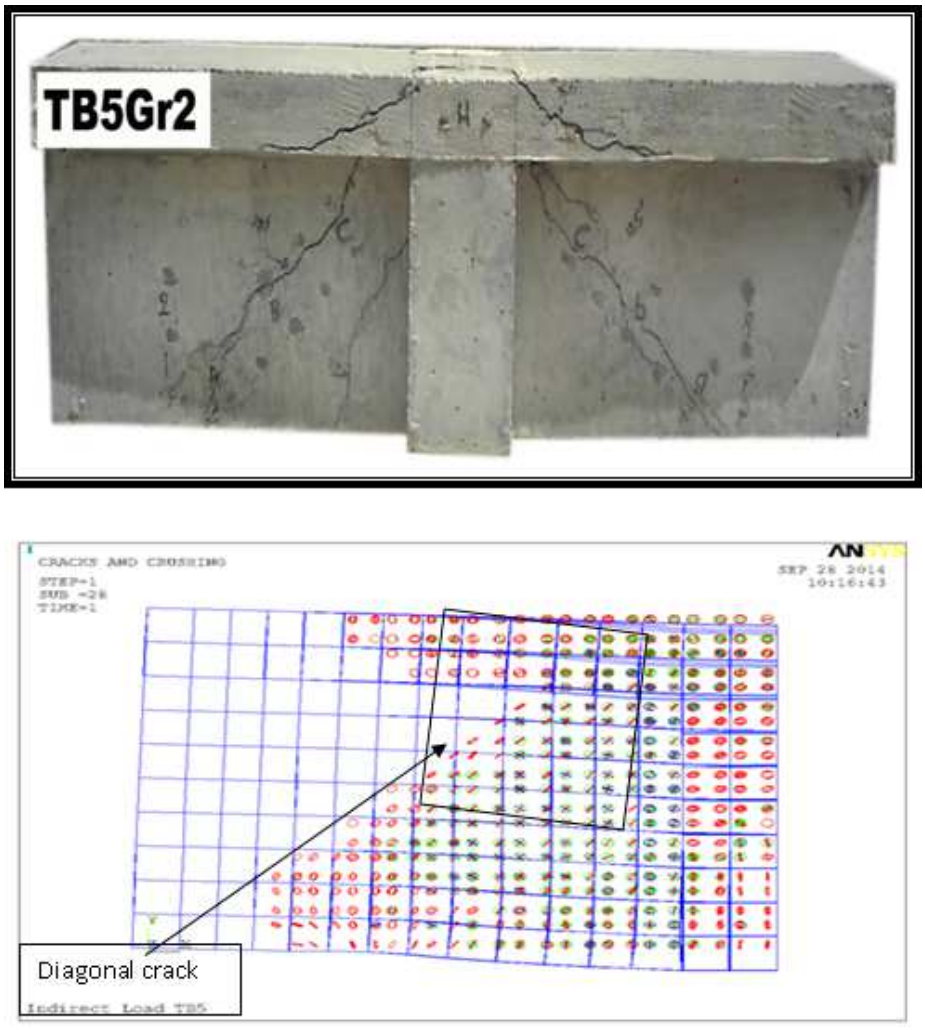

Figure 17: Crack Patterns at Ultimate Load as observed during Experiments and FE Analysis

CONCLUSIONS

The behaviors of indirectly loaded deep beams are examined through experiments and an FE model in this study. The results obtained are then compared. The tested beams are produced in a laboratory, and the beam model is loaded tothe point of failure.Deflection and crack patternsare monitored as well. FE behavior was analyzed using the ANSYS program. Eight-node (SOLID65) solid brick elements were used to model the concrete. Internal steel reinforcement was modeled using Link 8 3D spar elements.The ultimate load of failure and the displacement predicted by non-linear FE analysis are close to those measured during experimental testing. The load–mid-span deflection curves of the specimen from the FEANSYS analysis agreedwith theexperimentally obtained curves. The crack distributions observed in FE analysis also agreed with the experimental results. On the basis of the evaluation, the experimental results, and the FE analysis findings for indirectly loaded deep T-beams, the following conclusions can be drawn:

- The stresses and deflections at the centerline of cross sections andthe progressive cracking observed in the FE beam model are consistent withthose measured in a deep RC T-beam.

- The failure mechanism of indirectly loaded deep T-beams is effectively modeled through FE analysis. Moreover, the predicted ultimate failure load is close to that obtained during experimental testing.
- The crack pattern showed that the webs of all of the beams functioned as simple struts between loads and supports.
- The mid-span deflections of the indirectly loaded, flanged deep beams are smaller and fewer than the permissible deflections specified by ACI Building Code (318-11).These deflections did not cause any problem at service load Pu/1.5.
- The increase in flange size enhances the cracking and failure load- carrying capacity.The enlargement of flanges also reduces the corresponding mid-span deflection at the same a/d ratio.
- Both ultimate and inclined cracking loads tend to increase with a decrease in a/d ratio to below 1.8.

GENERAL SYMBOLS

Table 4

Symbol	Definition
hf	Flange depth
bf	Flange width
a	Shear span
b_w	Web width
h	Overall depth of beam
l	Clear span
P_{cr}	Cracking span load
P_u	Ultimate span load
d	Effective depth of beam
f_c'	Cylinder compressive strength of concrete
f_{cu}	Cube compressive strength of concrete

REFERENCES

1. Winter, G. and A.H. Nilson, Design of concrete structures. 1972: McGraw-Hill.
2. Park, R., Reinforced concrete structures. 1975: John Wiley & Sons.
3. Fereig, S. and K. Smith. Indirect loading on beams with short shear spans. in ACI Journal Proceedings. 1977. ACI.
4. Nawy, E.G., Reinforced Concrete: A Fundamental Approach (Prentice-Hall International Series In Civil Engineering And Engineering Mech. 1985.
5. Standard, A.A., Building Code Requirements for Structural Concrete (ACI 318-11). 2011.
6. Heywood, R., R. Pritchard, and P. Shaw, ASSESSMENT OF BRIDGES–CHALLENGING THE STRUCTURAL ENGINEERING PROFESSION.
7. Ferguson, P.M. Some implications of recent diagonal tension tests. in ACI Journal Proceedings. 1956. ACI.
8. Taylor, R., Some shear tests on reinforced concrete beams without shear reinforcement*. Magazine of Concrete

Research, 1960. 12(36): p. 145-154.

9. Taub, J. and A. Neville. Resistance to shear of reinforced concrete beams. in ACI Journal Proceedings. 1960. ACI.
10. Kalyanaraman, V., M.A. Rayan, and H.-Y. Pao, Shear tests of deep beams with flanges. Journal of the Structural Division, 1979. 105(12): p. 2760-2766.
11. Kong, F.K., Reinforced concrete deep beams. 2006: CRC Press.
12. Mohammadhassani, M., et al., Failure modes and serviceability of high strength self compacting concrete deep beams. Engineering Failure Analysis, 2011. 18(8): p. 2272-2281.
13. Committee, A. Building code requirements for structural concrete (ACI 318-05) and commentary (ACI 318R-05). 2005. American Concrete Institute.
14. Denpongpan, T., Effect of Reversed Loading on Shear Behavior of Reinforced Concrete, 2001, Kochi University of Technology.
15. Hawkins, N. and Chmn. Suggested revision to shear provisions for building code, by the ASCE-ACI Task Committee 426 on shear and Diagonal Tension. in ACI Journal Proceedings. 1977. ACI.
16. Smith, K. and S. Fereig, Effect of Loading and Supporting Conditions on the Shear Strength of Deep Beams. ACI Special Publication, 1974. 42.
17. Zhang, N. and K.-H. Tan, Size effect in RC deep beams: Experimental investigation and STM verification. Engineering structures, 2007. 29(12): p. 3241-3254.
18. C39, A., Standard Test Method for Compressive Strength of Cylindrical Concrete Specimens. 2010.
19. 1983, B.S.P., Methods for Determination of Compressive Strength of Concrete Cubes. 1983.
20. Syroka-Korol, E. and J. Tejchman, Experimental investigations of size effect in reinforced concrete beams failing by shear. Engineering Structures, 2014. 58: p. 63-78.
21. Omeman, Z., M. Nehdi, and H. El-Chabib, Experimental study on shear behavior of carbon-fiber-reinforced polymer reinforced concrete short beams without web reinforcement. Canadian Journal of Civil Engineering, 2008. 35(1): p. 1-10.
22. Shah, R. and S. Mishra, Crack and deformation characteristics of SFRC deep beams. Journal of the Institution of Engineers. India. Civil Engineering Division, 2004. 85(mai): p. 44-48.
23. Husain M. Husain, B.S.A.-N.m., Ali H. Aziz, Shear Behavior of Hybrid Reinforced Concrete I-Beams Containing Steel Fiber Reinforced Concrete (SFRC) and High Strength Concrete (HSC). Journal of Engineering and Development, 2006. Vol. 10 (No. 4): p. 36-52.
24. 426, A.-A.C. The shear strength of reinforced concrete members. in ACI Journal Proceedings. 1973. ACI.
25. ANSYS, C., Help Manual 12.1.
26. Wolanski, A.J., Flexural behavior of reinforced and prestressed concrete beams using finite element analysis,

2004, Citeseer.

27. Kachlakev, D., et al., Finite Element Modeling of Concrete Structures Strengthened with FRP Laminates. Final report, SPR, 2001. 316.
28. Ibrahim, A.M. and M.S. Mahmood, Finite element modeling of reinforced concrete beams strengthened with FRP laminates. European journal of scientific research, 2009. 30(4): p. 526-541.
29. Hemmaty, Y. Modeling of the shear force transferred between cracks in reinforced and fiber reinforced concrete structures. in Proceedings of the ANSYS Conference. 1998.
30. Willam, K. and E. Warnke. Constitutive model for the triaxial behavior of concrete. in Proceedings, International Association for Bridge and Structural Engineering. 1975. ISMES, Bergamo, Italy.
31. Desayi, P. and S. Krishnan. Equation for the stress-strain curve of concrete. in ACI Journal Proceedings. 1964. ACI.
32. Gere, J. and S. Timoshenko, Mechanics of materials. 1997. PWS Pub. Co., Boston.
33. Fanning, P., Nonlinear models of reinforced and post-tensioned concrete beams. Electronic Journal of Structural Engineering, 2001. 1: p. 111-119.
34. Al-Manaseer, A. and D. Phillips, Numerical study of some post-cracking material parameters affecting nonlinear solutions in RC deep beams. Canadian Journal of Civil Engineering, 1987. 14(5): p. 655-666.
35. y Certificación, A.E.d.N., Eurocode 3: Design of steel structures–Part 1-1: General rules and rules for buildings. UNE-EN, 1993: p. 1-1.
36. Hawileh, R., et al., Modeling of insulated CFRP-strengthened reinforced concrete T-beam exposed to fire. Engineering Structures, 2009. 31(12): p. 3072-3079.
37. Özcan, D.M., et al., Experimental and finite element analysis on the steel fiber-reinforced concrete (SFRC) beams ultimate behavior. Construction and Building Materials, 2009. 23(2): p. 1064-1077.